



Figures and figure supplements

Imaging neuropeptide release at synapses with a genetically engineered reporter

Keke Ding *et al*

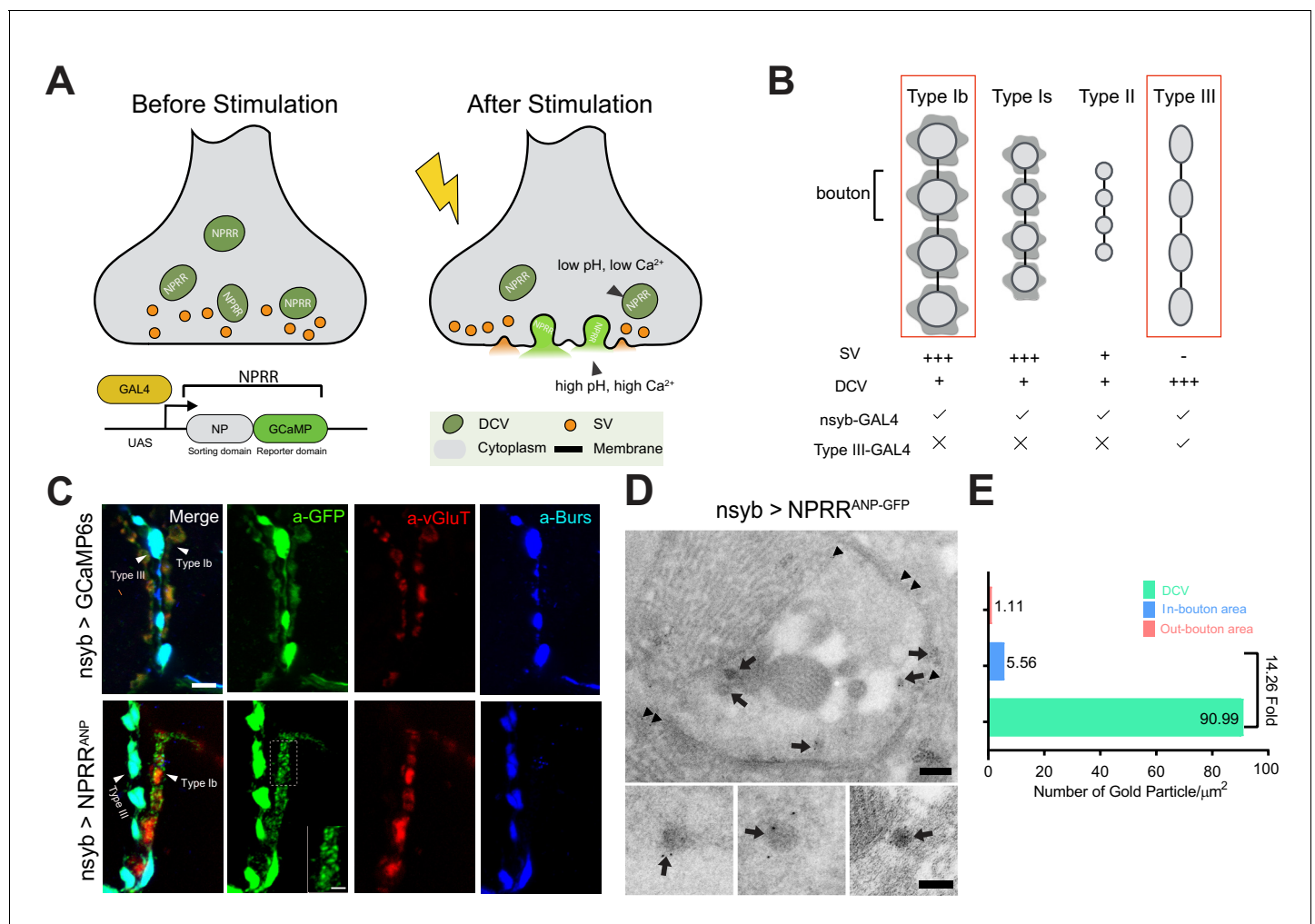


Figure 1. Design and Synaptic Localization of an NPRR. (A) Schematic illustrating the principle of NPRRs (Neuropeptide Release Reporters). NPRR molecules in the DCV lumen (low pH/low calcium, left) exhibit increased fluorescence when released by fusion into the extracellular space (neutral pH/high calcium, right). NPRR fluorescent signal is expected to decay following diffusion into the synaptic cleft. New NPRR-containing DCVs are produced by synthesis and transport from the soma, not by recycling. NP: Neuropeptide. DCV: Dense Core Vesicle. SV: Synaptic Vesicle. (B) Distinct motor neuron subtypes at the *Drosophila* NMJ (muscle 12/13) have different proportions of DCVs vs. SVs. The GAL4 driver R57C10-Gal4 (nsyb-GAL4) labels all subtypes, while R20C11-GAL4 selectively labels only Type III neurons, which lack SVs ('Type III-GAL4'). Light gray circles, black lines and dark gray shading represent boutons, inter-bouton intervals and subsynaptic reticulum respectively. The studies in this paper focus on Type Ib neurons and Type III neurons (in red rectangles). (C) Triple immunolabeling for GFP (green), Bursicon (blue) and vGluT (red), in flies containing nsyb-GAL4 driving UAS-GCaMP6s (upper), or NPRR^{ANP} (lower). Type Ib and Type III boutons are indicated. Scale bar, 5 μ m. Inset image (NPRR^{ANP}, a-GFP channel) shows details of puncta distribution of NPRR^{ANP} in Type Ib neuron. Scale bar, 2 μ m. (D) TEM images of boutons immunolabeled with anti-GFP (5 nm gold particle-conjugated) to detect nsyb>NPRR^{ANP-GFP}, which has an identical structure to NPRR^{ANP}, but is a GFP rather than GCaMP6s fusion to improve antigenicity (see Figure 1—figure supplement 4). Note strong labeling in DCVs (arrows) and the neuronal plasma membrane (arrowheads). Scale bar, 200 nm. Lower panel shows representative images of labeled DCVs. Scale bar, 100 nm. (E) Quantification for TEM images in (D).

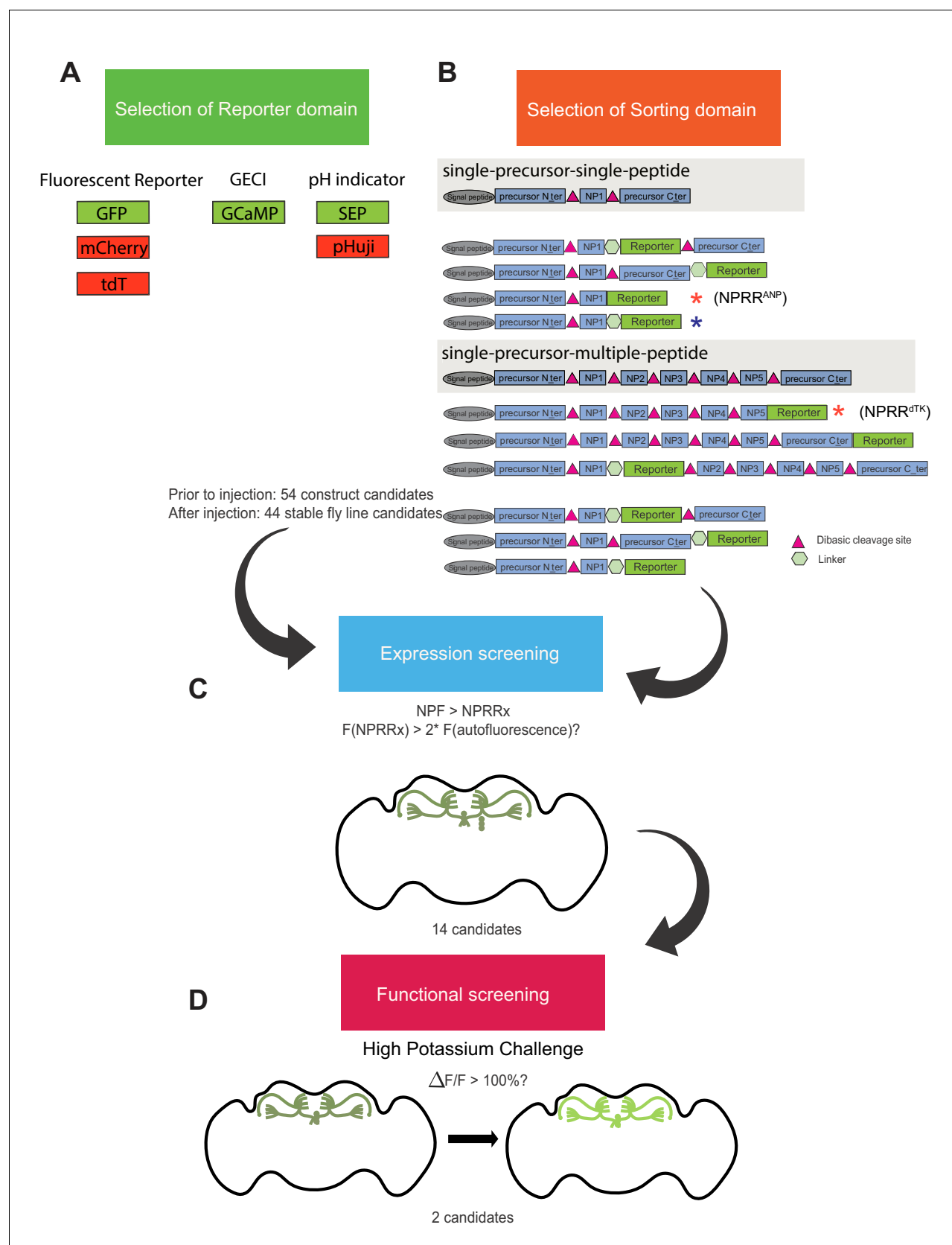


Figure 1—figure supplement 1. NPRR screening pipeline. A series of reporter-neuropeptide precursor fusions were designed, codon-optimized for *Drosophila*, cloned into expression vectors under the control of the GAL4 upstream activator sequence (UAS), and used to generate transgenic flies. (A) Figure 1—figure supplement 1 continued on next page

Figure 1—figure supplement 1 continued

Candidate reporters interrogated included (constitutive) fluorescent reporters, genetically encoded calcium indicators (GECI) and pH indicators (pHluorins). (B) Sorting domain candidates included different truncated versions of rat Atrial Natriuretic Peptide (ANP; single-precursor-single-peptide) and *Drosophila* tachykinin (dTK; single-precursor-multiple-peptide) precursors. 52 constructs were built and injected. 44 of 54 were successfully integrated as transgenic lines, while eight were excluded due to lethality or unstable expression. (C–D) Candidate UAS-NPRR lines were crossed with an NPF-Gal4 driver line and selected based on their expression in NPF terminals in the adult fly brain. The raw fluorescence intensity of each NPRR candidate was measured using the same microscope parameters (laser power, HV, offset value). 14 candidates passed this screening. (C) We screened the performance of difference NPRRs (signal-to-noise contrast) by measuring fluorescence before and immediately after 70 mM high-potassium challenge in an ex vivo explant preparation of adult fly brains. The post/pre KCl fluorescence ratio is defined as $\Delta F/F$. We arbitrarily set the threshold as 100%. 2 NPRRs with highest $\Delta F/F$ passed the final round of screening. Red asterisks indicate the candidates selected for the studies in **Figure 2** and **Figure 3**. Blue asterisk indicates original ANP-GFP fusion (*Burke et al., 1997; Rao et al., 2001*).

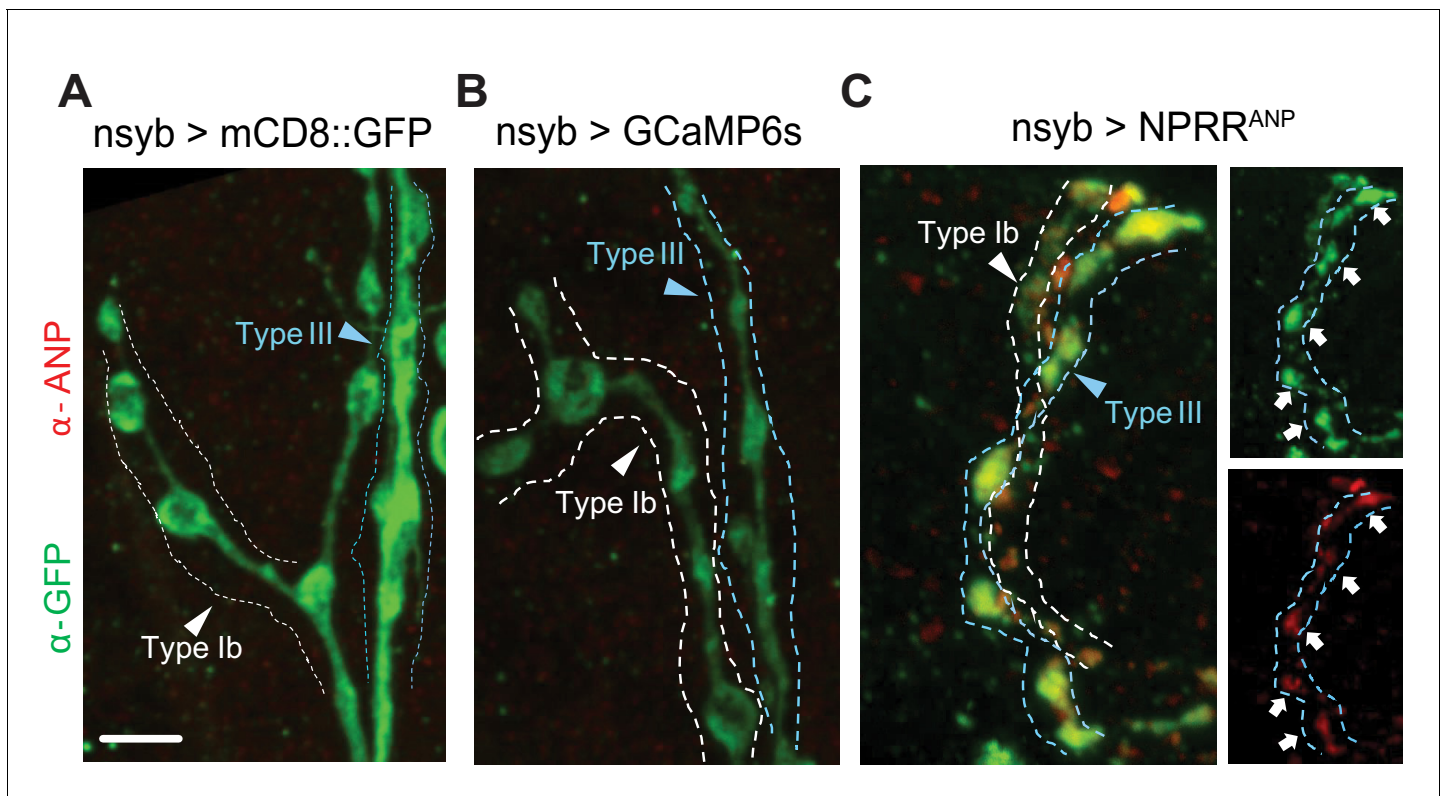


Figure 1—figure supplement 2. Exogenous neuropeptide ANP dictates the expression pattern of $NPRR^{ANP}$. Membrane-bound $mCD8::GFP$ fusion (A), cytosolic $GCaMP6s$ (B) and $NPRR^{ANP}$ (C) were expressed pan-neuronally in the larval NMJ and stained for both ANP (red) and $NPRR$ (green, anti-GFP). (C) Note co-localization of ANP and GFP. Scale bar, 5 μm .

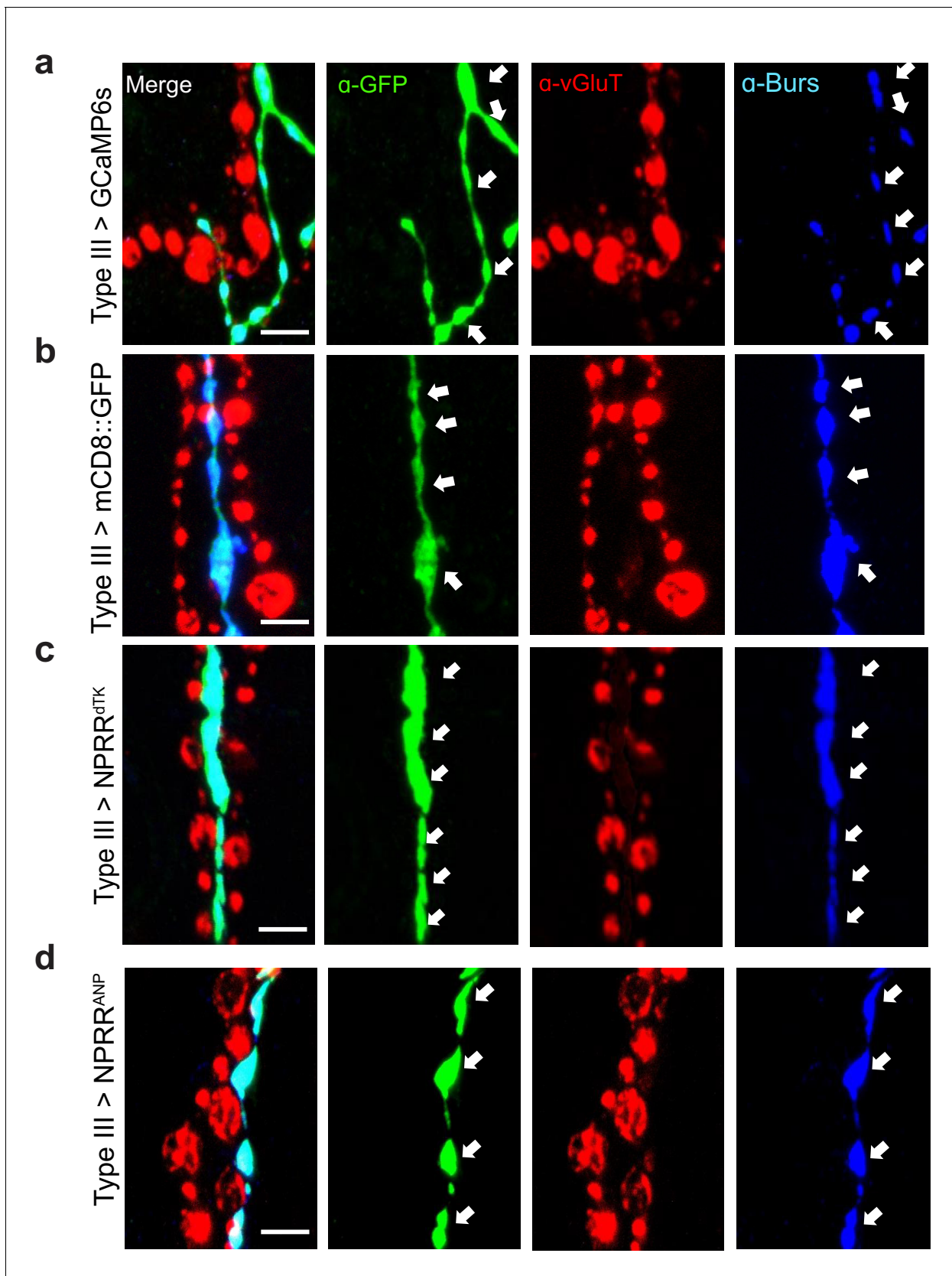


Figure 1—figure supplement 3. Expression of different reporters in Type III neurons in the larval NMJ. A GAL4 line (R20C11-GAL4, named Type III-GAL4 in this report) allows specific expression in Type III neurons. Expression patterns of (A) conventional GCaMP, (B) membrane-bound GFP, (C) Figure 1—figure supplement 3 continued on next page

Figure 1—figure supplement 3 continued

NPRR^{dTK} and (D) NPRR^{ANP} using Type III-GAL4. Arrows indicate boutons in Type III neurons, which contain the neuropeptide Bursicon. Note that anti-vGluT stains other types of motor neurons, which are not labeled by the Type III-specific driver used in this experiment. Scale bar, 5 μ m.

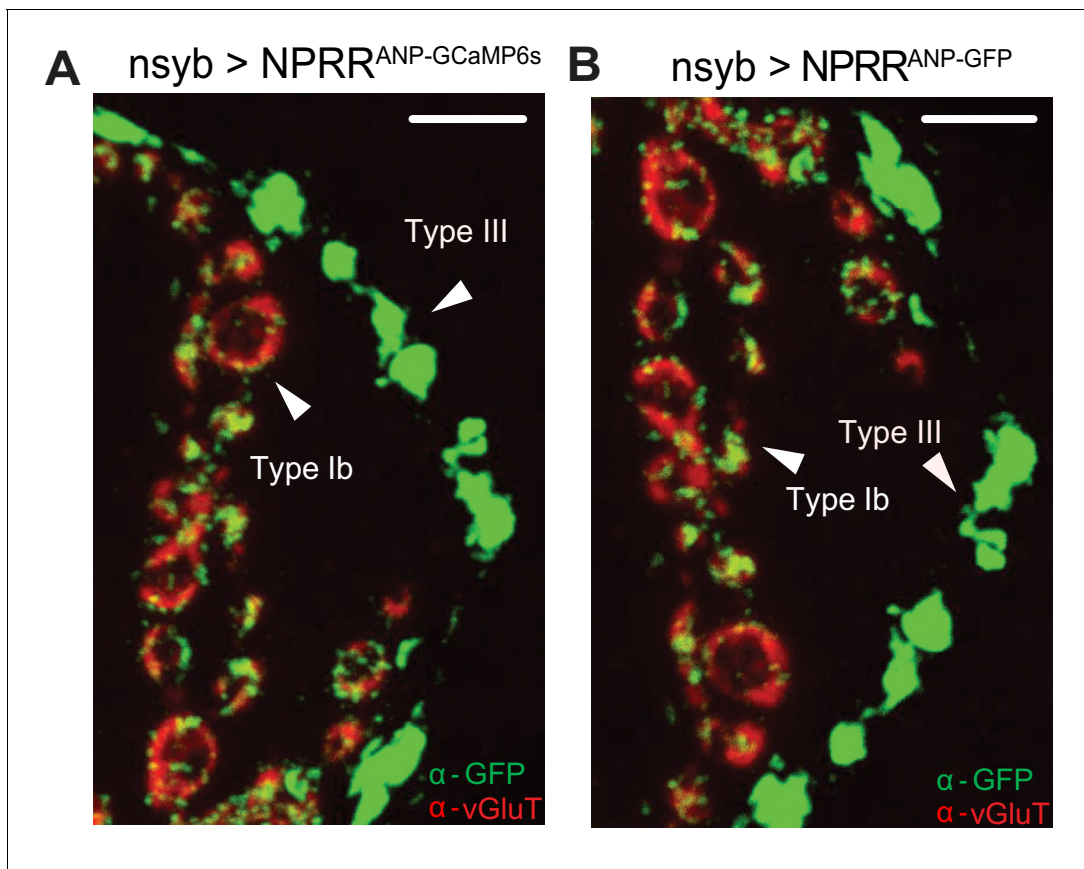


Figure 1—figure supplement 4. Subcellular distribution of NPRR^{ANP} and NPRR^{ANP-GFP}. NPRR^{ANP} (labeled as NPRR^{ANP-GCaMP6s}) (A) and NPRR^{ANP-GFP} (B) were expressed pan-neuronally in the larval NMJ and double immune-labeled with antibodies to vGluT (red) and GFP (green). Note that the distribution of GFP signal is similar whether the reporter fusion is GCaMP6s (A) or GFP (B). Scale bar, 5 μm.

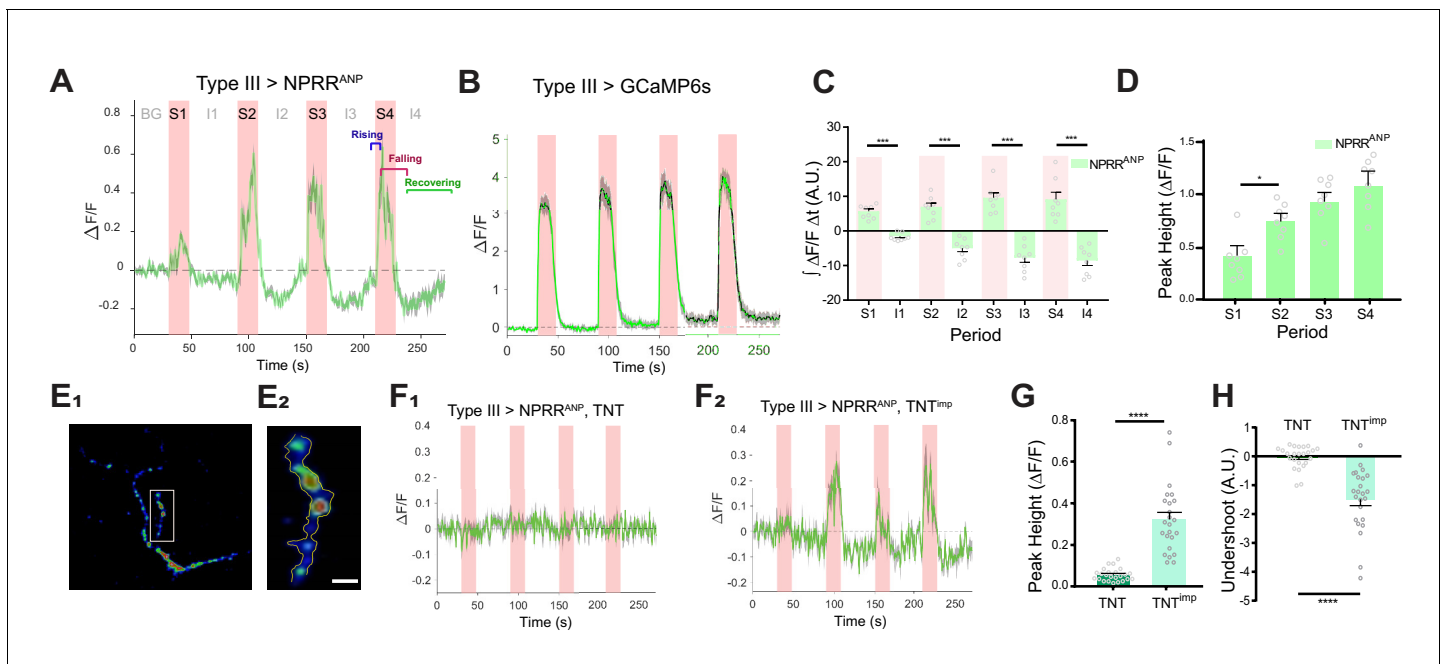


Figure 2. NPRR specifically reports neuropeptide release. (A) Trace from a representative experiment showing changes in NPRR^{ANP} fluorescence intensity ($\Delta F/F$) in Type III motor neurons at the larval NMJ evoked by electrical stimulation. BG: background. S1-S4: Stimulation trials 1–4. I1-I4: Interstimulation Intervals (ISIs) 1–4. Green line: $\Delta F/F$ averaged across all boutons in the field of view. Gray shading: s.e.m. envelope. Red bar: electrical stimulation trials (70 Hz). The three typical phases of the response are indicated in S4. The peak height of the response on the first trial is characteristically lower (see also (D)), and may reflect competition with unlabeled DCVs in the readily releasable pool. (B) $\Delta F/F$ traces in control flies expressing cytoplasmic GCaMP6s in Type III neurons. (C) Integrated NPRR^{ANP} $\Delta F/F$ values during trials S1-4 and intervals I1-4. A.U.: arbitrary units. $n = 8$. ***, $p < 0.001$. (D) Average NPRR^{ANP} $\Delta F/F$ peak heights for trials S1-4. $n = 8$. *, $p < 0.05$. Plotted values in (C–D) are mean \pm s.e.m. (E₁–E₂) Representative selection of ROIs (yellow). Details see Materials and methods. Scale bar, 5 μ m. (F) NPRR^{ANP} $\Delta F/F$ response are abolished in Type III GAL4>UAS NPRR^{ANP} flies bearing UAS-TNT (F₁) but not UAS-TNT^{imp} (F₂). (G) Average peak heights of NPRR^{ANP} $\Delta F/F$ in combined stimulation trials (S1-4) from (F). ****, $p < 0.0001$. (H) Average 'undershoot', defined as the integrated $\Delta F/F$ during ISIs I1-4 (see (C)). In (C–D) and (G–H).

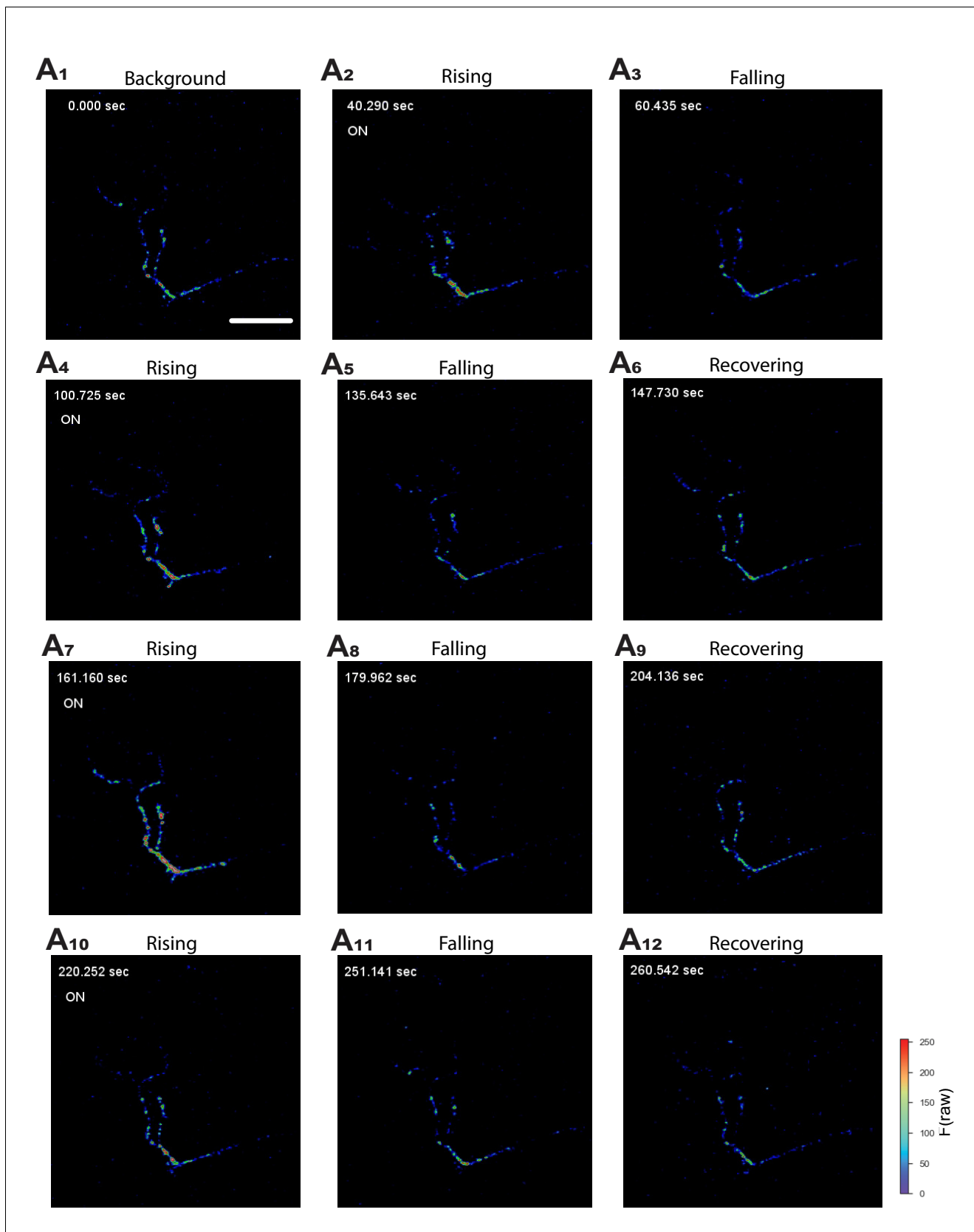


Figure 2—figure supplement 1. Activation of NPRR^{ANP} in situ. Representative still frames (A₁–A₁₂) from video recordings of NPRR^{ANP}-expressing Type III neurons at the larval NMJ. 'On' (A_{2,4,7,10}) represents the onset of electrical pulses. Color bar: Raw fluorescence intensity. Scale bar, 50 μm.

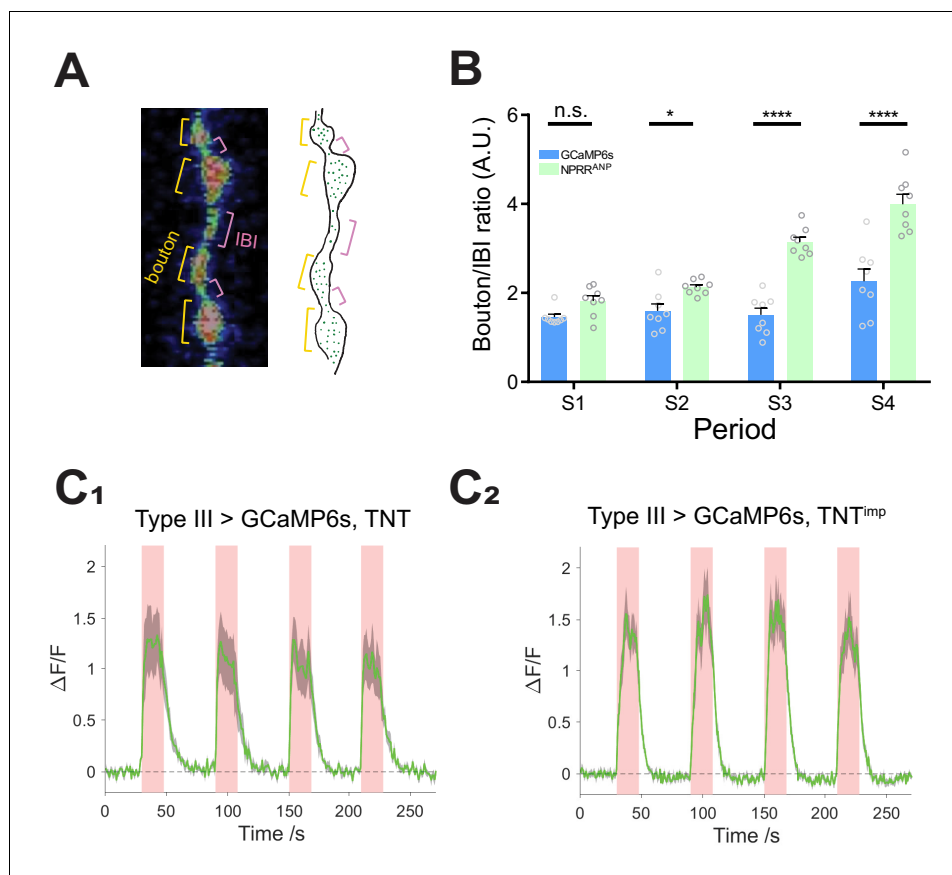


Figure 2—figure supplement 2. NPPR specifically reports neuropeptide release. (A) Left: Segmentation of Type III neurons into boutons (orange) and inter-bouton intervals (IBIs, red). Right: Schematic illustrating DCV distribution in Type III neurons, based on photomicrograph to the left. Green dots, DCVs. (B) Average time-integrated ratio of $\Delta F/F$ in boutons/IBIs (Materials and Methods), within each stimulation periods. n.s., not significant. *, $p < 0.05$. ***, $p < 0.001$. ****, $p < 0.0001$. (C) TNT does not affect GCaMP6s $\Delta F/F$ kinetics. $n = 6-7$. GCaMP6s peak magnitudes were reduced slightly in TNT (C₁) in comparison to TNT^{imp} (C₂) preparations, perhaps reflecting partial vulnerability of the cytosolic GCaMP6s reporter to TNT-mediated cleavage and degradation. NPPRs are expected to be protected from TNT by the DCV membrane.

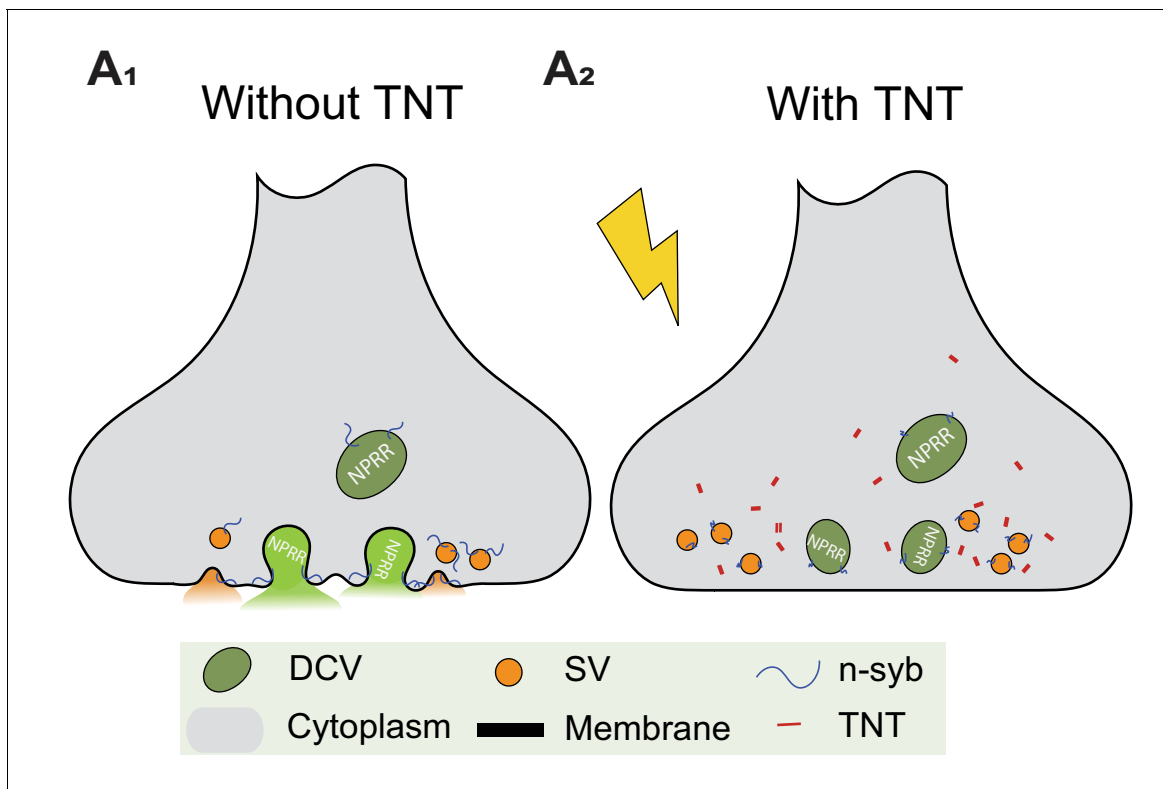


Figure 2—figure supplement 3. Blocking DCV fusion using Tetanus Toxin. (A₁, A₂) Tetanus toxin (TNT) blocks vesicle fusion by cleavage of n-synaptobrevin (n-syb).

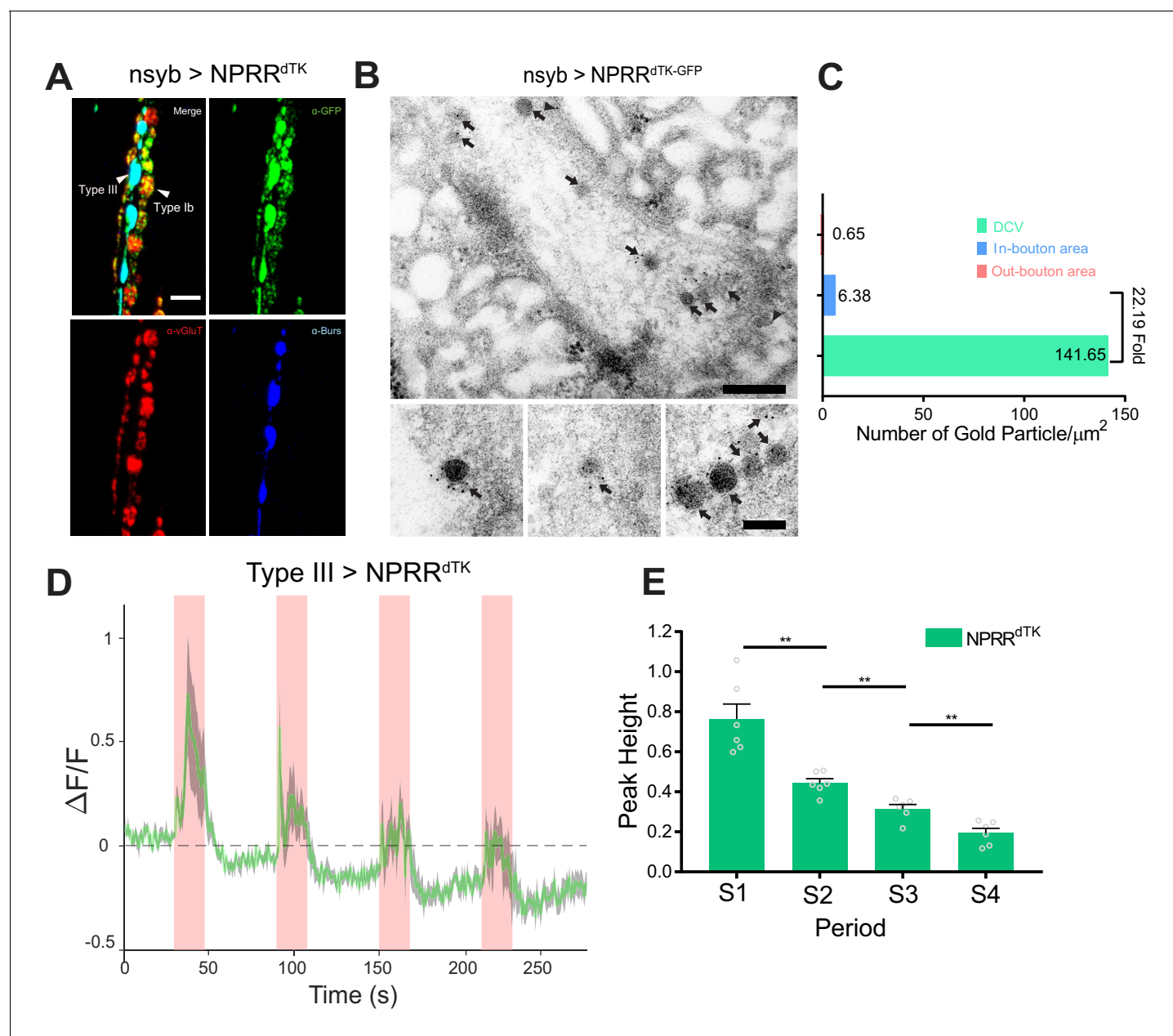


Figure 3. Application of the NPRR approach to a *Drosophila* neuropeptide. (A) Triple immunolabeling for GFP (green), Bursicon (blue) and vGluT (red) in Type III-GAL4 > UAS NPRR^{dTK} flies. Scale bar, 5 μm. (B) TEM images of boutons immunolabeled against GFP (5 nm gold) in nsyb-GAL4 > UAS NPRR^{dTK-GFP} flies. Note strong labeling in DCVs (arrows) and bouton plasma membrane (arrowheads). Scale bar, 200 nm. Lower panel shows representative images of labeled DCVs. Scale bar, 100 nm. (C) Quantification of TEM images in (B). (D) NPRR^{dTK} ΔF/F curve; stimulation conditions as in Figure 2A. (E) Average NPRR^{dTK} ΔF/F peak height above pre-stimulation baseline (corrected; see Materials and methods) for stimulation trials S1-4. *n* = 6. **, *p* < 0.01.

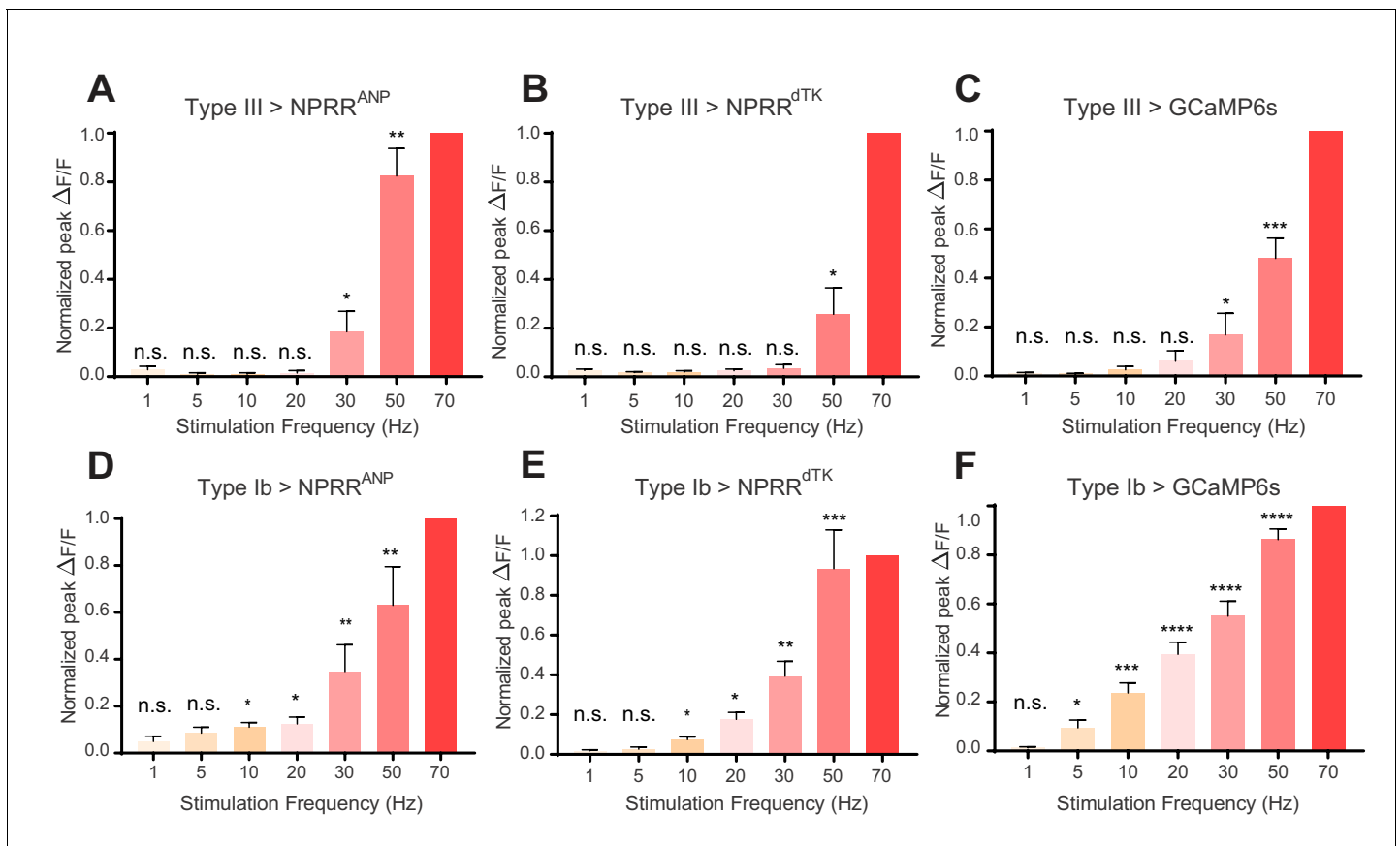


Figure 4. NPRR reveals distinct cell-type specific peptide release properties. For each preparation, a series of stimulation trials were delivered at frequencies from 1 Hz to 70 Hz, as indicated. In-stimulation response peaks were normalized to 70 Hz. The normalized peaks of NPRRs or calcium responses (measured with cytosolic GCaMP6s) were pooled and plotted for both Type III (A-C) and Type Ib (D-F) neurons. Responses were compared to zero. $n = 6-12$. n.s., not significant. *, $p < 0.05$. **, $p < 0.01$. ***, $p < 0.001$. ****, $p < 0.0001$.

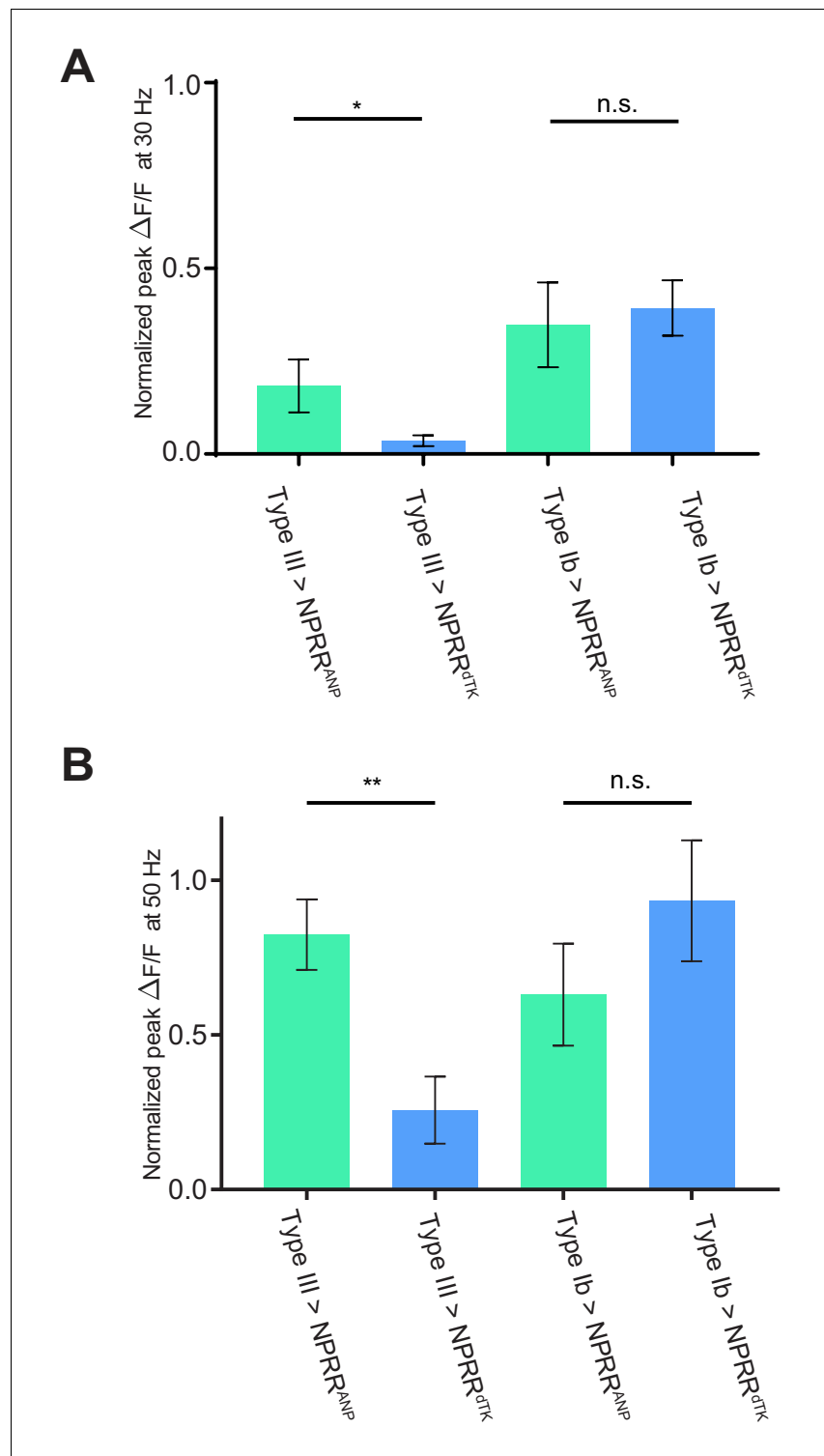


Figure 4—figure supplement 1. Comparison of NPRR response at 30 and 50 Hz. Normalized $\Delta F/F$ peaks in at 30 Hz (A) and 50 Hz (B) electrical stimulation in **Figure 4A,B,D,E** are replotted and compared. $n = 6-7$. *, $p < 0.05$. **, $p < 0.01$. n.s., not significant.